PCCP

PAPER

View Article Online
View Journal | View Issue

Cite this: *Phys. Chem. Chem. Phys.*, 2023, **25**, 28063

Hydration makes a difference! How to tune protein complexes between liquid–liquid and liquid–solid phase separation†

Sashary Ramos, [a] Janine Kamps, [b] Simone Pezzotti,[a] Konstanze F. Winklhofer,[c] Jörg Tatzelt [b] and Martina Havenith *[ad]

Understanding how protein rich condensates formed upon liquid–liquid phase separation (LLPS) evolve into solid aggregates is of fundamental importance for several medical applications, since these are suspected to be hot-spots for many neurotoxic diseases. This requires developing experimental approaches to observe in real-time both LLPS and liquid–solid phase separation (LSPS), and to unravel the delicate balance of protein and water interactions dictating the free energy differences between the two. We present a vibrational THz spectroscopy approach that allows doing so from the point of view of hydration water. We focus on a cellular prion protein of high medical relevance, which we can drive to undergo either LLPS or LSPS with few mutations. We find that it is a subtle balance of hydrophobic and hydrophilic solvation contributions that allows tuning between LLPS and LSPS. Hydrophobic hydration provides an entropic driving force to phase separation, through the release of hydration water into the bulk. Water hydrating hydrophilic groups provides an enthalpic driving force to keep the condensates in a liquid state. As a result, when we modify the protein by a few mutations to be less hydrophilic, we shift from LLPS to LSPS. This molecular understanding paves the way for a rational design of proteins.

Received 12th July 2023,
Accepted 1st September 2023

DOI: 10.1039/d3cp03299j

rsc.li/pccp

1. Introduction

Cellular compartmentalization and spatiotemporal control of biochemical reactions have been longstanding questions in cell biology. Cells contain membrane-defined compartments, or organelles, that can physically segregate cellular regions. Additionally, membrane-less compartments, such as stress granules, nucleolus, and P-bodies, have also been observed and garnered much interest in recent years. Evidence suggests that liquid–liquid phase separation (LLPS), also referred to as condensate formation, plays a vital role in the construction of membrane-less bodies.[1–4] Biomolecular condensates can rapidly form upon stimulation and be dissolved when their function is completed. They can serve as reaction centers for biochemical processes or storage centers for biomolecules under stress conditions. Interestingly, many proteins that can undergo LLPS contain intrinsically disordered regions (IDRs) or low complexity domains (LCDs) that enable multivalent interactions. Recently, it has been evident that many pathogenic proteins linked to neurodegenerative disease can undergo LLPS *in vitro* and *in cellulo*.[3,5–7] This has led to a hypothesis that the formation of biomolecular condensates through LLPS precedes the formation of pathogenic protein aggregates through liquid–solid phase separation (LSPS). Therefore, understanding the mechanism of LLPS and LSPS and the transition between the two are prominent challenges for biological and medical applications.

Tackling this challenge requires experimental techniques that can monitor LLPS, LSPS, and the maturation of condensates in real time and unravel the delicate balance of protein–protein, protein–water, and water–water interactions dictating their free energy.[8–13] While the protein–protein effects and protein conformational changes have been extensively investigated, the driving forces behind such phase-separation processes are not fully understood. In particular, the contribution of hydration enthalpy and entropy to the process of LLPS has often been neglected so far. Nevertheless, hydration free energies do provide key driving forces to LLPS,[11,13–17] as well as to LSPS.[18–21]

Recently, we introduced a spectroscopic approach that can quantify the solvation-based driving forces associated with

[a] *Department of Physical Chemistry II, Ruhr University Bochum, Bochum, Germany. E-mail: martina.havenith@rub.de*
[b] *Department of Biochemistry of Neurodegenerative Diseases, Institute of Biochemistry and Pathobiochemistry, Ruhr University Bochum, Bochum, Germany*
[c] *Department of Molecular Cell Biology, Institute of Biochemistry and Pathobiochemistry, Ruhr Unviersity Bochum, Bochum, Germany*
[d] *Department of Physics, TU Dortmund, Dortmund, Germany*

† Electronic supplementary information (ESI) available. See DOI: https://doi.org/10.1039/d3cp03299j

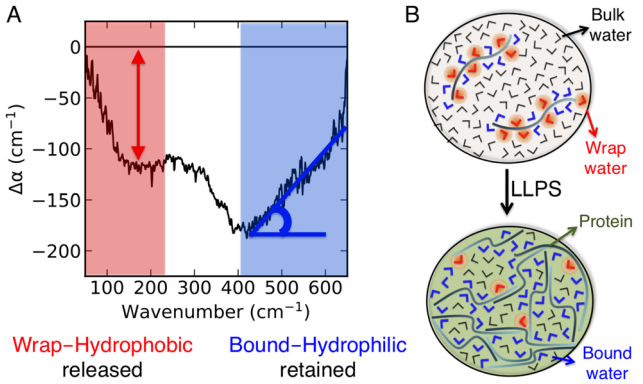

Fig. 1 THz signatures of LLPS. (A) A typical example of difference THz spectrum upon LLPS. In our approach,[8,11] THz spectra are measured as a function of time during LLPS, and difference THz spectra are constructed by subtracting the initial spectrum (*i.e.* measured before LLPS takes place) from the spectrum recorded subsequent to LLPS. The two characteristic hydration water signatures of LLPS, *i.e.* the negative band at ~150 cm^{-1} (red, as quantified by the negative amplitude) and the $\Delta\alpha$ (almost linear) increase in the 450–650 cm^{-1} range (blue, as quantified by the associated slope, $\Delta\alpha/\Delta\nu$), are highlighted. (B) Molecular sketches illustrating the corresponding hydration populations: cavity-wrap water hydrating hydrophobic patches is released upon LLPS, giving rise to a loss of the ~150 cm^{-1} band, while bound water hydrating hydrophilic groups is retained, causing an increase in the slope ($\Delta\alpha/\Delta\nu$) in the cm^{-1} range.

LLPS; this method directly correlates signatures in the low-frequency vibrational THz spectrum (50–650 cm^{-1}) of the phase-separated system to solvation free energies.[8,11] The THz range is ideal for probing changes in the hydration water network,[22–30] and the spectra can be deconvoluted so that they specifically report on how hydration changes upon LLPS.[8] A typical example is illustrated in Fig. 1. It shows two characteristic features due to local hydration water changes upon LLPS, as described in details in ref. 8, 22, 27 and 31:

• A negative amplitude in the 100–250 cm^{-1} spectral region, due to the distortion of the water H-bond network that wraps around the cavity that hosts the protein. This feature is due to hydrophobic hydration, *i.e.* cavity formation, and referred to as cavity-wrap.

• An almost linear $\Delta\alpha$ increase in the librational part of the THz spectrum, from 450 to 650 cm^{-1}, which is assigned to bound water hydrating hydrophilic moieties. For bound water, the steric constraints in water rotational motions induced by the proximity to and direct H-bonding with the solutes cause a reduction in the amplitude of soft librational modes and an increase in that of hard librations, resulting in a characteristic $\Delta\alpha$ linear increase in the >400 cm^{-1} frequency range.[31,32]

The combination of these two observables is characteristic of the occurrence of LLPS.[8,11] In order to understand what makes the difference between forming either liquid condensates or solid aggregates, we here focus on the cellular prion protein (PrP), which can be driven to undergo LLPS *vs.* LSPS with few mutations.[33] Based on our results, we can state that it is a subtle balance of hydrophobic and hydrophilic solvation contributions that is decisive. Very interestingly, such balance can be tuned by *ad hoc* designed modifications of the amino acid sequence, as in the case of PrP.

2 Results and discussion

N1 but not N1ΔPB undergoes LLPS

We have recently shown that the intrinsically disordered domain of the mammalian prion protein undergoes LLPS.[33] In particular, only the N1 domain of PrP (N1PrP) is necessary for the formation of protein condensates. Further, removing the polybasic motifs in the N1 domain impedes the formation of liquid-like droplets and rather gel-like or aggregated assemblies are formed (LSPS). N1ΔPB, a variant in which lysines and arginines in the polybasic motifs (PB) 1 and 2 were mutated to alanines, formed undynamic protein aggregates indicative of LSPS.[33] The amino acid sequence and modifications are shown in Fig. 2A. The different behavior between N1 and N1ΔPB is illustrated in the volumetric three-dimensional reconstitutions and fluorescence recovery after photobleaching experiments (FRAP) recordings shown in Fig. 2B.

THz observables for hydration contributions to LLPS *vs.* LSPS

We hereafter use the novel THz-calorimetry technique to decipher the effect of the mutations on the protein's hydration entropy and enthalpy. Difference THz Spectroscopy in an attenuated total reflection geometry was used to capture the distinct hydration of the protein undergoing either LLPS or LSPS. For comparison, Fig. 2C displays difference THz spectra between final (after LLPS) and initial (before LLPS) states of a time series of THz measurements (see methods for details). Example spectra of a full time series are shown in the ESI.† They report on the hydration water contributions that change upon phase separation.[8]

The N1 PrP difference spectrum shows two absorption features reporting on hydrophobic (at lower frequency, red) and hydrophilic (at higher frequency, blue) hydration contributions upon LLPS. Strikingly, a much different spectral shape is observed for the N1ΔPB PrP variant that undergoes LSPS. This result already indicates that hydration water plays very different roles in LLPS and LSPS processes, and that THz spectroscopy sensitively captures these differences. Specifically, both difference spectra display a negative $\Delta\alpha$ contribution from the release of wrap water at lower frequency, albeit much weaker in the case of the N1ΔPB PrP variant. What is truly remarkable, however is the distinctive hydration signatures in the frequency range where the bound water (hydrophilic) hydration population is probed. For N1 PrP, $\Delta\alpha$ increases (almost linearly) with frequency above 400 cm^{-1}, a clear signature of the presence of bound water within the condensates. In contrast, $\Delta\alpha$ decreases in the same frequency range for N1ΔPB PrP, indicating a loss of bound water. This demonstrates that the hydrophilic hydration contribution upon phase separation yields an opposite trend in the cases of LLPS and LSPS, *i.e.* it is the discriminant hydration contribution among the two processes. The specific contributions from hydrophobic and hydrophilic hydration can be quantified by the THz-phase diagram that we recently introduced for LLPS in ref. 8, as shown in Fig. 3. The axes of the diagram specifically report on the changes of the cavity-wrap and bound THz observables during phase separation. To quantify the hydrophobic cavity-wrap water contribution (*x*-axis), the amplitude of the negative band at ~150 cm^{-1} is used. For the hydrophilic bound water

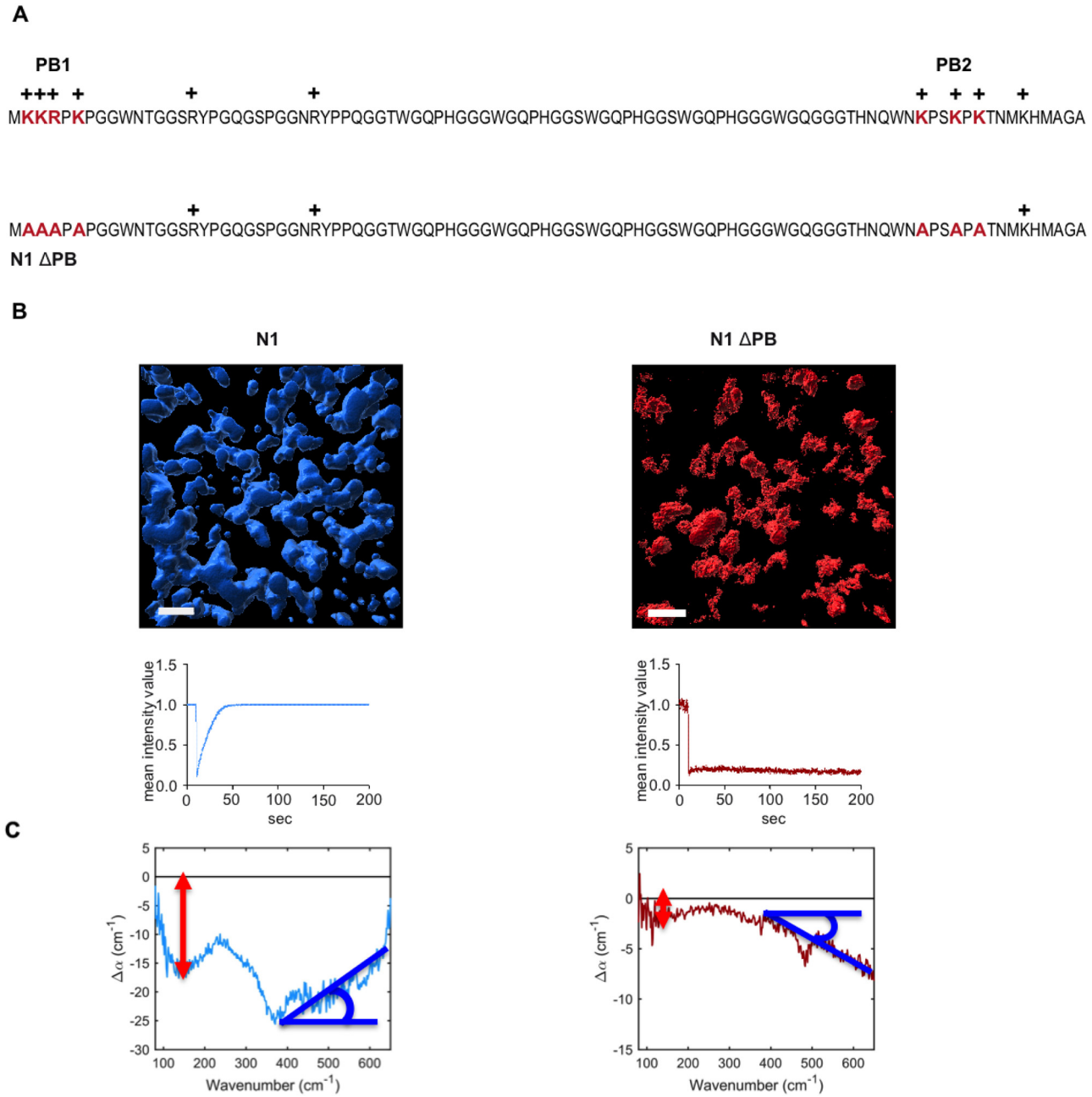

Fig. 2 (A) Amino acid sequence (one letter code) of N1 and N1ΔPB (PB, polybasic cluster). (B) volumetric three-dimensional reconstitution using Z-stack images (volume of 67.5 × 67.5 × 10 μm) from confocal laser scanning microscopy (upper panels, scale bar represents 10 μm). Fluorescence recovery after photobleaching (FRAP) was used to detect the protein mobility within the condensates (lower panels). (C) Average difference spectra generated by the subtraction of the first spectrum obtained in the measurement series (no LLPS) from the final spectrum obtained at 60 min in the measurement series (LLPS). The N1-PrP (blue) displays stronger LLPS signatures than the N1ΔPB (red). Interestingly, the contribution of bound water at high frequency displays an opposite slope between the two PrP variants.

contribution (y-axis) we use the slope ($\Delta\alpha/\Delta\nu$) obtained by linearly fitting the $\Delta\alpha$ increase/decrease in the 400–650 cm^{-1} frequency range, previously demonstrated to be the best choice to quantify the contribution in a robust and transferable way.[8,27,28,31,32,34] Each point in the THz phase diagram corresponds to a measured sample. Non phase-separating systems provide points close to (0,0), by construction. For comparison, the points obtained for the present two systems (red and light blue) are reported in Fig. 3 together with several previously studied systems (grey points) undergoing LLPS (from ref. 8 and 11).

Notably, all systems undergoing LLPS are inscribed in the same quadrant of the THz phase diagram, corresponding to negative $\Delta\alpha$ (wrap) and positive $\Delta\alpha$ (bound) values. As it is already known, these values are due to (i) cavity-wrap water hydrating hydrophobic patches of the protein surfaces that is released outside of the condensates, into the diluted phase

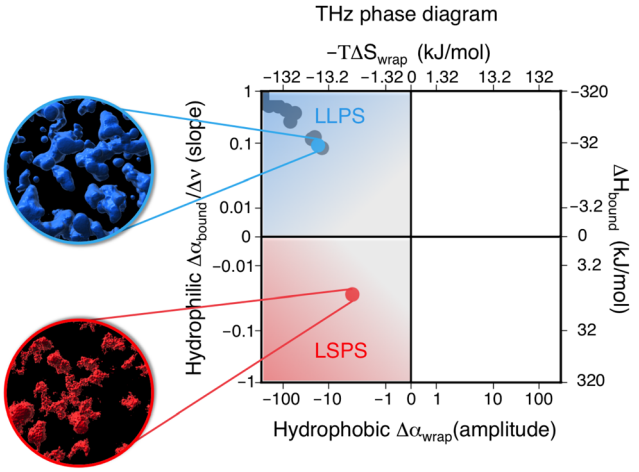

Fig. 3 Thz phase-diagram showing the correlation between bound (*y*-axis) and cavity-wrap (*x*-axis) water contributions to phase separation (LLPS *vs.* LSPS), as well as the associated entropic and enthalpic driving forces as quantified by means of eqn (2). The blue point shows the correlation between bound water and cavity-wrap water for N1, while in red is that of the N1ΔPB. The grey points correspond to previous measurements of systems undergoing LLPS, from ref. 8 and 11. Protein solutions prior to phase separation correspond to the (0,0) point, by construction. The upper quadrant (blue) is associated with LLPS, where we see a gain in bound water paired with a loss of cavity-wrap water,[8] while the lower quadrant (red) is associated with LSPS, where there is a loss of both bound and cavity-wrap water.

upon LLPS; (ii) bound water hydrating hydrophilic patches that is retained as much as possible into the condensates. While the sign of the wrap and bound contributions are common for all LLPS systems, the absolute values show a variance that depends on the nature of the protein, temperature, concentration, *etc.*[8]

The striking result is that the N1-PrP mutant undergoing LSPS is contained in a different quadrant of the diagram, where both Δα (wrap) and Δα (bound) are negative. This result has two important implications. First, it proves that our spectroscopic approach allows to discriminate between LLPS and LSPS based on spectroscopic observables. Second, it means that upon LSPS both water hydrating hydrophilic and hydrophobic patches are released into the liquid bulk.

A hydration entropy/enthalpy balance keeps the condensates liquid

The entropic and enthalpic driving forces that give rise to the different behavior of hydration water upon LLPS and LSPS can be rationalized directly from the measured THz spectra thanks to the THz-calorimetry approach. We previously showed[8,31] that the hydration contributions to Δ*H* and Δ*S* upon phase separation can be quantitatively expressed as a sum of hydrophobic and hydrophilic contributions from the cavity-wrap and bound spectroscopic populations, respectively:

$$\begin{aligned}\Delta G^{\text{hydration}}_{\text{LLPS}} &= \Delta H^{\text{hydration}}_{\text{LLPS}} - T\Delta S^{\text{hydration}}_{\text{LLPS}}\\ \Delta S^{\text{hydration}}_{\text{LLPS}} &= \Delta S_{\text{cavity}} + \Delta S_{\text{bound}}\\ \Delta H^{\text{hydration}}_{\text{LLPS}} &= \Delta H_{\text{cavity}} + \Delta H_{\text{bound}}\end{aligned} \quad (1)$$

The partial ΔS_{cavity} hydrophobic contribution is expected to dominate the hydration entropy changes, while the ΔH_{bound} contribution is most relevant for hydration enthalpy,[8,20,31,35] Therefore, in the following we will focus on ΔS_{cavity} and ΔH_{bound}, only. In order to quantify these partial free energy terms, we use the following linear correlation functions with the measured cavity-wrap ($\Delta\alpha_{\text{wrap}}$) and bound ($\Delta\alpha_{\text{bound}}/\Delta\nu$) water spectroscopic observables:[8,31]

$$\begin{aligned}\Delta S^{\text{hydration}}_{\text{LLPS}} \simeq \Delta S_{\text{cavity}} &= \Delta\alpha_{\text{wrap}}\Delta\bar{S}_{\text{wrap}},\\ \Delta\bar{S}_{\text{wrap}} &= -4.4\,\text{J mol}^{-1}\,\text{K}^{-1}\,\text{cm}\\ \Delta H^{\text{hydration}}_{\text{LLPS}} \simeq \Delta H_{\text{bound}} &= \Delta\alpha_{\text{bound}}/\Delta\nu\Delta\bar{H}_{\text{bound}},\\ \Delta\bar{H}_{\text{bound}} &= -320\,\text{kJ mol}^{-1}\,\text{cm}\end{aligned} \quad (2)$$

where $\Delta\alpha_{\text{wrap}}$ and $\Delta\alpha_{\text{bound}}$ are plotted in the diagram of Fig. 3 (we remind the reader that $\Delta\alpha_{\text{bound}}$ is measured as a slope, therefore the nomenclature $\Delta\alpha_{\text{bound}}/\Delta\nu$), while $\Delta\bar{S}_{\text{wrap}}$ and $\Delta\bar{H}_{\text{bound}}$ are constant correlation factors that we previously obtained based on a large set of solutes.[22,31] The concept beyond this set of equations is that the variations in the local hydration water network that dictate hydration entropy and enthalpy are fully encoded in the spectroscopic response of hydration water in the low frequency THz range. Therefore, such constant correlation factors are general and system independent, as detailed in previous works.[31,32,36]

The negative sign of $\Delta\bar{S}_{\text{wrap}}$, combined with the negative amplitude, *i.e.* $\Delta\alpha_{\text{wrap}} < 0$ of the wrap spectroscopic population, already tells us that the release of cavity-wrap water into the diluted phase provides a hydration driving force for phase separation, as it increases the entropy. This result is in agreement with previous theoretical[37] and experimental studies[8,11] on different protein solutions, showing the generality of our finding. Therefore, it is now evident why our spectra show $\Delta\alpha_{\text{wrap}} < 0$ for both LLPS and LSPS: the entropic driving force from hydrophobic hydration is mandatory to have favorable solvation contributions to phase separation. Based on these results we can more generally propose that if a protein is too hydrophilic, there will be not enough cavity-wrap water to release and the solvation contribution to phase-separation would be unfavorable.

By contrast, the bound water contribution disfavors phase separation, since $\Delta\bar{H}_{\text{bound}} < 0$ implies that releasing bound waters to create protein–protein interactions requires an enthalpic penalty. However, such enthalpic penalty from hydrophilic hydration is the driving force to retain water within the condensates formed upon LLPS and keep them in a liquid, reversible state. This driving force depends on the amount of hydrophilic groups on the protein surface that can form strong interactions with bound water. Having removed the hydrophilic polybasic domain in the mutated N1PrP, the enthalpic driving for retaining bound waters is dramatically reduced. We can quantify the magnitude of such reduction based on the THz observable. By plugging the measured $\Delta\alpha_{\text{bound}}$ (slope) values into eqn (2), we find that the enthalpic driving force is reduced by 35.2 kJ mol^{-1} (= 14 $k_{\text{B}}T$) for the mutated prion protein. Our

experimental evidence that LSPS instead of LLPS takes place for the mutated N1 PrP demonstrates that this 35.2 kJ mol^{-1} is sufficient to disfavor the retain of bound water and shift the phase separation equilibrium from LLPS to LSPS.

3 Conclusion

The final picture obtained from our novel THz spectroscopic approach (THz-calorimetry) is summarized in Fig. 4. We find that LLPS involves a tight balance of hydrophobic and hydrophilic hydration contributions. The hydrophobic solvation contribution is mandatory to have a favorable solvation driving force for LLPS, *i.e.* solvation will disfavor LLPS for a too hydrophilic protein. Nevertheless, we also find that tuning the balance too much on the hydrophobic side shifts the phase-separation equilibrium from LLPS toward LSPS. These hydration contributions upon phase separation are captured by a THz-phase diagram: The axes quantify the hydrophobic and hydrophilic hydration observables, which are quantitatively correlated to entropic and enthalpic driving forces by means of eqn (2). As a consequence of the balance/imbalance of both hydration contributions, LLPS and LSPS appear in different quadrants of the diagram. Interestingly, for the investigated prion protein, we can state that just the presence *vs.* lack of bound waters differentiate between LLPS and LSPS, by providing an enthalpic driving force of as much as 35 kJ mol^{-1} to keep the condensates in liquid *vs.* solid state.

These results pave the way toward rationally tuning the hydrophobic–hydrophilic hydration balance to either induce or prevent LLPS *vs.* LSPS, by choosing specific mutations of the prion protein. We expect this will benefit the many biological and medical efforts to prevent LSPS as well as condensate maturation into solid aggregates.

4 Experimental

Expression and purification

Plasmid and proteins were maintained, expressed and purified as previously described.[33] Briefly, PrP constructs were based on the coding region of the mouse PrP gene (Prnp: GenBank accession number M18070) and modified to express PrP-L108M/V111M.[38] The N1 construct consists of residues 23 to 114. The modified N1 construct, N1ΔPB, has had lysines and arginines in both polybasic motifs modified to alanines. Both constructs were expressed in BL21-DE3 strains and induced with 100 μM IPTG when the cells reached an absorbance (600 nm) of 0.9. Proteins were stored in 50 mM Na_2HPO_4/NaH_2PO_4 (pH 8.0), 500 mM NaCl, 0.01 mM $ZnCl_2$, 5% glycerol at −80 °C until further use.

Sample preparation for microscopy and THz spectroscopy

All experiments were conducted with the protein in 10 mM Tris, pH 7.4. Buffer exchange was done using Vivaspin 500 columns with a 30 kDa molecular weight cut off (Sartorius Stedim Biotech). The protein was then centrifuged five times for 7 minutes at 4 °C and 12 000 g. The concentration was measured with a NanoDrop2000 (Thermo Scientific) before use. To induce phase separation of the protein, TEV protease was added to each sample and incubated at room temperature for 1 hour. Samples were measured immediately after TEV cleavage.

Laser scanning microscopy

Fluorescent imaging laser scanning microscopy was performed on a microscope (ELYRA PS.1; Carl Zeiss) with an imaging detector (LSM 880; Carl Zeiss) as previously described.[11,33] A stack of 67.5 × 67.5 × 10 μm and 0.9 μm for each optical section was recorded with a 63× numerical aperture 1.4 oil-immersion

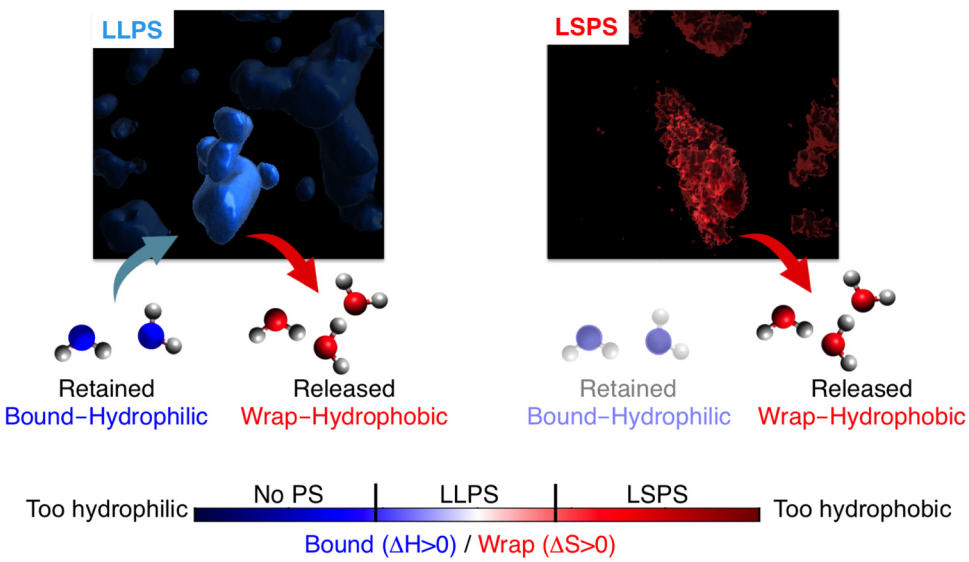

Fig. 4 Our results reveal that LLPS is favored by solvation only for a tight balance of hydrophobic and hydrophilic hydration contributions. Both release of (hydrophobic) cavity-wrap water and retain of (hydrophilic) bound water provide essential driving forces for LLPS, which are entropic and enthalpic, respectively. A too hydrophilic protein lacks the hydrophobic entropic driving force to phase separate, while a too hydrophobic protein misses the enthalpic driving force to retain bound water, shifting the phase separation balance toward LSPS instead of LLPS.

objective for Z-stack scanning. The Argon laser power was 0.006% at 488 nm with pixel dwell time of 5.71 μs. These settings were kept constant during all measurements. For 3-D reconstitution of the Z-stack images, the surface model from Imaris 9.3.1 was used. FRAP experiments were performed using ZEN2.1 bleaching region software module Plan-Apochromat 100× numerical aperture 1.46 oil-differential interference contrast M27 objective. The regions of interest were three circular areas with a 12-pixel diameter. Two regions were used as reference and background signal. The third region was bleached with 100% laser power, a pixel dwell time of 8.71 ms, with a scan time of 111.29 ms and a pixel dwell time of 1.61 ms. Data was analyzed in Excel 2016 and diagrams were generated with GraphPad Prism.

Fourier transform THz spectroscopy

FT-THz spectra were collected on an Bruker Vertex 80v FT-IR (Bruker, Billerica, MA) spectrometer using a liquid-Helium-cooled silicon bolometer (Infrared Laboratories, Tucson, AZ) as a detector. The sample compartment was equipped with a room-temperature single-reflection ATR MVP-Pro unit (Harrick Scientific, Pleasantville, NY) containing a diamond prism (2 × 3 mm). The sample (20 μL) was deposited on the diamond crystal and measured for 60 min at intervals of 2 minutes, resulting in a total of 30 spectra per sample. The time series chosen ensures that after 60 min the endpoint of the measurements is reached, *i.e.* when most of the volume probed is condensates formed from LLPS, see all details in ref. 36 Upon LLPS formation, the denser LLPS droplets sink to the bottom of the ATR unit, and are probed by the evanescent fields in FTIR-ATR. Spectra are recorded continuously until no further changes are observed. At this time the ATR probing depth is fully covered with the droplets or aggregates that are formed. The observed continuous increase in both absorption features related to phase separation is used as an experimental check for the stability in the spectrometer, spectra are thus recorded every 2 minutes. The difference spectrum shows the difference between the initial spectrum (solvated protein solution) and the final spectrum of the protein enriched condensates. All spectra were collected as an average of 64 scans and spectral resolution of 2 cm^{-1}. Only the initial (t = 0 min) and final (t = 60 min) spectra were used for analysis.

For analysis, the ATR absorption coefficient, α, was calculated using eqn (3),

$$\alpha(\nu) = -\frac{1}{d_p}\ln\left(\frac{I(\nu)}{I_0(\nu)}\right) \quad (3)$$

where d_p is the frequency-dependent penetration depth, $I(\nu)$ is the intensity of the sample, and $I_0(\nu)$ is the intensity of the reference, in this case the clean diamond crystal. The penetration depth was calculated by taking into account the refractive indices of the diamond crystal, $n_{diamond}$, and of the sample, n_{sample} using eqn (4).

$$d_p = \frac{\lambda}{2\pi\sqrt{{n_{diamond}}^2 \sin(\theta)^2 - {n_{sample}}^2}} \quad (4)$$

Where λ is the wavelength of the incident light and θ is the incident angle (45°). The refractive index of diamond was set at a constant value of 2.38 and that of the sample was set to 1.5. The refractive index of the sample was assumed to be the average of water at this frequency range for the sake of simplicity. All data shown here, and all analysis was conducted on difference absorption spectra, $\Delta\alpha$, which were calculated by subtracting the spectrum at t = 0 min from subsequent spectra, as shown in eqn (5)

$$\Delta\alpha = \alpha_{final} - \alpha_{initial} \quad (5)$$

where α_{final} is the spectrum collected at t = 60 min.

Conflicts of interest

There are no conflicts to declare.

Acknowledgements

We thank Benedikt König for fruitful discussions. The authors acknowledge funding by the Deutsche Forschungsgemeinschaft (DFG, German Research Foundation) under Germanys Excellence Strategy – EXC2033 – 390677874 – RESOLV. S. R. acknowledges funding from the European Union's Horizon 2020 programme (FP-RESOMUS – MSCA 801459). This work is supported by the ''Center for Solvation Science ZEMOS'' funded by the German Federal Ministry of Education and Research BMBF and by the Ministry of Culture and Research of Nord Rhine-Westphalia MKW NRW.

References

1 S. F. Banani, H. O. Lee, A. A. Hyman and M. K. Rosen, Biomolecular condensates: organizers of cellular biochemistry, *Nat. Rev. Mol. Cell Biol.*, 2017, **18**, 285–298.
2 B. Monterroso, S. Zorrilla, M. Sobrinos-Sanguino, C. D. Keating and G. Rivas, Microenvironments created by liquid-liquid phase transition control the dynamic distribution of bacterial division FtsZ protein, *Sci. Rep.*, 2016, **6**, 1–13.
3 Y. Shin and C. P. Brangwynne, Liquid phase condensation in cell physiology and disease, *Science*, 2017, **357**, eaaf4382.
4 A. R. Strom, A. V. Emelyanov, M. Mir, D. V. Fyodorov, X. Darzacq and G. H. Karpen, Phase separation drives heterochromatin domain formation, *Nature*, 2017, **547**, 241–245.
5 A. Patel, H. O. Lee, L. Jawerth, S. Maharana, M. Jahnel, M. Y. Hein, S. Stoynov, J. Mahamid, S. Saha and T. M. Franzmann, *et al.*, A liquid-to-solid phase transition of the ALS protein FUS accelerated by disease mutation, *Cell*, 2015, **162**, 1066–1077.
6 L. Guo, H. J. Kim, H. Wang, J. Monaghan, F. Freyermuth, J. C. Sung, K. O'Donovan, C. M. Fare, Z. Diaz and N. Singh, *et al.*, Nuclear-import receptors reverse aberrant phase transitions of RNA-binding proteins with prion-like domains, *Cell*, 2018, **173**, 677–692.
7 M. Hofweber, S. Hutten, B. Bourgeois, E. Spreitzer, A. Niedner-Boblenz, M. Schifferer, M.-D. Ruepp, M. Simons, D. Niessing and T. Madl, *et al.*, Phase separation of FUS is suppressed by its

nuclear import receptor and arginine methylation, *Cell*, 2018, **173**, 706–719.
8 S. Pezzotti, B. König, S. Ramos, G. Schwaab and M. Havenith, Liquid–Liquid Phase Separation? Ask the Water!, *J. Phys. Chem. Lett.*, 2023, **14**, 1556–1563.
9 D. Dimitrijevic, M. Bösenhofer and M. Harasek, Liquid–Liquid Phase Separation of Two Non-Dissolving Liquids—A Mini Review, *Processes*, 2023, **11**, 1145.
10 A. Ianiro, H. Wu, M. M. van Rijt, M. P. Vena, A. D. Keizer, A. C. C. Esteves, R. Tuinier, H. Friedrich, N. A. Sommerdijk and J. P. Patterson, Liquid–liquid phase separation during amphiphilic self-assembly, *Nat. Chem.*, 2019, **11**, 320–328.
11 J. Ahlers, E. M. Adams, V. Bader, S. Pezzotti, K. F. Winklhofer, J. Tatzelt and M. Havenith, The key role of solvent in condensation: mapping water in liquid-liquid phase-separated FUS, *Biophys. J.*, 2021, **120**, 1266–1275.
12 H. Cinar and R. Winter, The effects of cosolutes and crowding on the kinetics of protein condensate formation based on liquid–liquid phase separation: a pressure-jump relaxation study, *Sci. Rep.*, 2020, **10**, 1–16.
13 P. Pyne and R. K. Mitra, Excipients do regulate phase separation in lysozyme and thus also its hydration, *J. Phys. Chem. Lett.*, 2022, **13**, 931–938.
14 O. Fisette, C. Päslack, R. Barnes, J. M. Isas, R. Langen, M. Heyden, S. Han and L. V. Schäfer, Hydration dynamics of a peripheral membrane protein, *J. Am. Chem. Soc.*, 2016, **138**, 1526–11535.
15 M. Tros, L. Zheng, J. Hunger, M. Bonn, D. Bonn, G. J. Smits and S. Woutersen, Picosecond orientational dynamics of water in living cells, *Nat. Commun.*, 2017, **8**, 1–7.
16 G. Reddy, J. E. Straub and D. Thirumalai, Dry amyloid fibril assembly in a yeast prion peptide is mediated by long-lived structures containing water wires, *Proc. Natl. Acad. Sci. U. S. A.*, 2010, **107**, 21459–21464.
17 S. Park, R. Barnes, Y. Lin, B.-J. Jeon, S. Najafi, K. T. Delaney, G. H. Fredrickson, J.-E. Shea, D. S. Hwang and S. Han, Dehydration entropy drives liquid-liquid phase separation by molecular crowding, *Commun. Chem.*, 2020, **3**, 1–12.
18 D. Chandler, Interfaces and the driving force of hydrophobic assembly, *Nature*, 2005, **437**, 640–647.
19 K. Lum, D. Chandler and J. D. Weeks, Hydrophobicity at small and large length scales, *J. Phys. Chem. B*, 1999, **103**, 4570–4577.
20 D. M. Huang and D. Chandler, Temperature and length scale dependence of hydrophobic effects and their possible implications for protein folding, *Proc. Natl. Acad. Sci. U. S. A.*, 2000, **97**, 8324–8327.
21 S. N. Jamadagni, R. Godawat and S. Garde, Hydrophobicity of proteins and interfaces: insights from density fluctuations, *Annu. Rev. Chem. Biomol. Eng.*, 2011, **2**, 147–171.
22 F. Bohm, G. Schwaab and M. Havenith, Mapping hydration water around alcohol chains by THz calorimetry, *Angew. Chem., Int. Ed.*, 2017, **56**, 9981–9985.
23 D. Ben-Amotz, Hydration-shell vibrational spectroscopy, *J. Am. Chem. Soc.*, 2019, **141**, 10569–10580.
24 A. J. Bredt and D. Ben-Amotz, Influence of crowding on hydrophobic hydration-shell structure, *Phys. Chem. Chem. Phys.*, 2020, **22**, 11724–11730.
25 C. Weeraratna, C. Amarasinghe, W. Lu and M. Ahmed, A direct probe of the hydrogen bond network in aqueous glycerol aerosols, *J. Phys. Chem. Lett.*, 2021, **12**, 5503–5511.
26 J. G. Davis, K. P. Gierszal, P. Wang and D. Ben-Amotz, Water structural transformation at molecular hydrophobic interfaces, *Nature*, 2012, **491**, 582–585.
27 V. Conti Nibali, S. Pezzotti, F. Sebastiani, D. R. Galimberti, G. Schwaab, M. Heyden, M.-P. Gaigeot and M. Havenith, Wrapping up hydrophobic hydration: locality matters, *J. Phys. Chem. Lett.*, 2020, **11**, 4809–4816.
28 S. Pezzotti, A. Serva, F. Sebastiani, F. S. Brigiano, D. R. Galimberti, L. Potier, S. Alfarano, G. Schwaab, M. Havenith and M.-P. Gaigeot, Molecular fingerprints of hydrophobicity at aqueous interfaces from theory and vibrational spectroscopies, *J. Phys. Chem. Lett.*, 2021, **12**, 3827–3836.
29 E. M. Adams, S. Pezzotti, J. Ahlers, M. Rüttermann, M. Levin, A. Goldenzweig, Y. Peleg, S. J. Fleishman, I. Sagi and M. Havenith, Local mutations can serve as a game changer for global protein solvent interaction, *JACS Au*, 2021, **1**, 1076–1085.
30 S. Ebbinghaus, S. J. Kim, M. Heyden, X. Yu, U. Heugen, M. Gruebele, D. M. Leitner and M. Havenith, An extended dynamical hydration shell around proteins, *Proc. Natl. Acad. Sci. U. S. A.*, 2007, **104**, 20749–20752.
31 S. Pezzotti, F. Sebastiani, E. P. van Dam, S. Ramos, V. C. Nibali, G. Schwaab and M. Havenith-Newen, Spectroscopic fingerprints of cavity formation and solute insertion as a measure of hydration entropic loss and enthalpic gain, *Angew. Chem., Int. Ed.*, 2022, e202203893.
32 D. Das Mahanta, D. R. Brown, S. Pezzotti, S. Han, G. Schwaab, M. S. Shell and M. Havenith, Local water structures govern the mixing thermodynamics of glycerol-water solutions, *Chem. Sci.*, 2023, **14**(26), 7381–7392.
33 J. Kamps, Y.-H. Lin, R. Oliva, V. Bader, R. Winter, K. F. Winklhofer and J. Tatzelt, The N-terminal domain of the prion protein is required and sufficient for liquid-liquid phase separation: A crucial role of the αβ-binding domain, *J. Biol. Chem.*, 2021, 297.
34 C. Y. Ma, S. Pezzotti, G. Schwaab, M. Gebala, D. Herschlag and M. Havenith, Cation enrichment in the ion atmosphere is promoted by local hydration of DNA, *Phys. Chem. Chem. Phys.*, 2021, **23**, 23203–23213.
35 E. Gallicchio, M. Kubo and R. M. Levy, Enthalpy- entropy and cavity decomposition of alkane hydration free energies: Numerical results and implications for theories of hydrophobic solvation, *J. Phys. Chem. B*, 2000, **104**, 6271–6285.
36 B. König, S. Pezzotti, S. Ramos, G. Schwaab and M. Havenith, Real time measure of solvation free energy changes upon liquid–liquid phase separation of α-Elastin, *Biophys. J.*, 2023, **123**, DOI: 10.1016/j.bpj.2023.07.023.
37 V. Bianco, G. Franzese and I. Coluzza, In silico evidence that protein unfolding is a precursor of protein aggregation, *Chem. Phys. Chem.*, 2020, **21**, 377–384.
38 K. F. Winklhofer, U. Heller, A. Reintjes and J. R. Tatzelt, Inhibition of Complex Glycosylation Increases the Formation of PrPsc, *Traffic*, 2003, **4**, 313–322.